Brief Article

PET Imaging of Fatty Acid Amide Hydrolase with [18F]DOPP in Nonhuman Primates

Benjamin H. Rotstein,[†,‡] Hsiao-Ying Wey,[‡,§] Timothy M. Shoup,[†,‡] Alan A. Wilson,[∥] Steven H. Liang,[†,‡] Jacob M. Hooker,*[,‡,§] and Neil Vasdev*[,†,‡]

[†]Division of Nuclear Medicine and Molecular Imaging & Center for Advanced Medical Imaging Sciences, Massachusetts General Hospital, Boston, Massachusetts 02114, United States

[‡]Department of Radiology, Harvard Medical School, Boston, Massachusetts 02114, United States

[§]Athinoula A. Martinos Center for Biomedical Imaging, Massachusetts General Hospital, Charlestown, Massachusetts 02129, United States

[∥]Research Imaging Centre, Centre for Addiction and Mental Health & Department of Psychiatry, University of Toronto, Toronto, Ontario M5T 1R8, Canada

S Supporting Information

ABSTRACT: Fatty acid amide hydrolase (FAAH) regulates endocannabinoid signaling. [11C]CURB, an irreversibly binding FAAH inhibitor, has been developed for clinical research imaging with PET. However, no fluorine-18 labeled radiotracer for FAAH has yet advanced to human studies. [18F]DOPP ([18F]3-(4,5-dihydrooxazol-2-yl)phenyl (5-fluoropentyl)carbamate) has been identified as a promising 18F-labeled analogue based on rodent studies. The goal of this work is to evaluate [18F]DOPP in nonhuman primates to support its clinical translation. High specific activity [18F]DOPP (5−6 Ci·μmol⁻¹) was administered intravenously (iv) to three baboons (2M/1F, 3−4 years old). The distribution and pharmacokinetics were quantified following a 2 h dynamic imaging session using a simultaneous PET/MR scanner. Pretreatment with the FAAH-selective inhibitor, URB597, was carried out at 200 or 300 μg/kg iv, 10 min prior to [18F]DOPP administration. Rapid arterial blood sampling for the first 3 min was followed by interval sampling with metabolite analysis to provide a parent radiotracer plasma input function that indicated ∼95% baseline metabolism at 60 min and a reduced rate of metabolism after pretreatment with URB597. Regional distribution data were analyzed with 1-, 2-, and 3-tissue compartment models (TCMs), with and without irreversible trapping since [18F]DOPP covalently links to the active site of FAAH. Consistent with previous findings for [11C]CURB, the 2TCM with irreversible binding was found to provide the best fit for modeling the data in all regions. The composite parameter λk_3 was therefore used to evaluate whole brain (WB) and regional binding of [18F]DOPP. Pretreatment studies showed inhibition of λk_3 across all brain regions (WB baseline: 0.112 mL/cm³/min; 300 μg/kg URB597: 0.058 mL/cm³/min), suggesting that [18F]DOPP binding is specific for FAAH, consistent with previous rodent data.

KEYWORDS: [18F]DOPP, fatty acid amide hydrolase, FAAH, positron emission tomography, PET, kinetic modeling
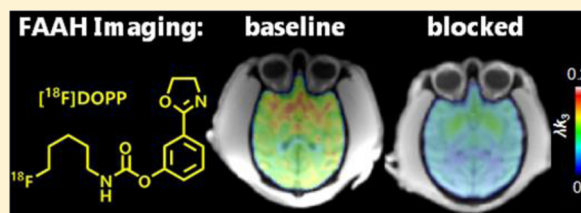
INTRODUCTION

Endocannabinoid signaling at the G-protein coupled receptors CB₁ and CB₂ is activated by the lipid messengers N-arachidonoylethanolamine (anadamide) and 2-arachidonoylglycerol (2-AG), which are metabolized by fatty acid amide hydrolase (FAAH) and monoacylglycerol lipase (MAGL), respectively.[1,2] Anandamide and 2-AG are thought to be produced on demand in postsynaptic neurons, since both chemical messengers have low aqueous solubility that may preclude vesicular storage.[3] Retrograde signaling to CB₁ on the presynaptic neurons then initiates a cascade that regulates calcium and potassium ion channels. Reuptake of endocannabinoids is still a matter of some debate, though it is believed to be preceded by amide hydrolysis, hence the tone of endocannabinoid signaling in the central nervous system is regulated by FAAH and MAGL.[4,5] Distortion in the cannabinoid system has been linked to a wide variety of pathologies including eating disorders, neurodegenerative disorders, anxiety, depression, pain, and inflammation.[6] FAAH in particular shows promise as a therapeutic target since selective inhibitors of this enzyme have not been shown to contribute to hypomotility, hyper-reflexia, and CB₁ receptor downregulation, nor to be candidates for substance abuse, in contrast to MAGL inhibitors.[7] Several FAAH inhibitors including URB597[8] and PF-04457845[9−12] (Figure 1) have

advanced to phase I and II clinical trials for treatment of pain, cannabis dependence, and schizophrenia.
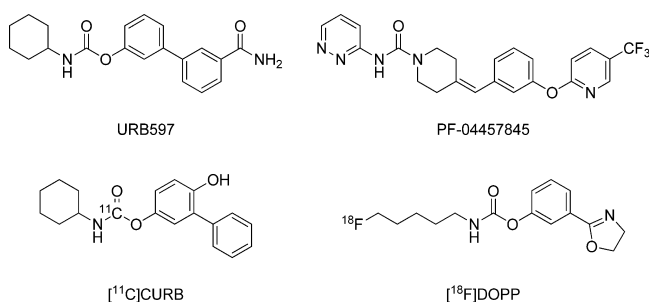
Figure 1. Structures of FAAH inhibitors URB597 and PF-04457845 and PET imaging agents [11C]CURB and [18F]DOPP.

Accurate quantification of FAAH activity in the living human brain under normal and diseased states would assist in understanding the role that the endocannabinoid system plays in these conditions, and could provide a valuable tool for drug development. Positron emission tomography (PET) is a noninvasive molecular imaging technique that uses positron-emitting radionuclides to prepare functional probes with high sensitivity and is administered at a dose that leads to minimal perturbation of the underlying biological state. Several PET radiotracers for FAAH have been reported, including anadamide analogues,[13] carbon-11 labeled PF-04457845[14] and a fluorine-18 labeled derivative,[15] [11C]MK-3168,[16] a 11C-*methyl* labeled URB597 analogue,[17] and related [11C-*carbonyl*]-O-arylcarbamates[18,19] prepared by 11CO2-fixation in the presence of an organic base.[20] Among PET radiotracers for FAAH, only two have been reported in human studies, namely [11C]MK-3168[21] and [11C-*carbonyl*]-6-hydroxy-[1,1'-biphenyl]-3-yl cyclohexylcarbamate ([11C]CURB).[18,22] We are evaluating [11C]CURB, which is an irreversible covalent inhibitor of FAAH. This scaffold has been fruitful for development of selective FAAH CNS probes due to the mechanism of inhibition by covalent modification of the Ser$_{241}$-Ser$_{217}$-Lys$_{142}$ active site, which is unusual for serine hydrolases.[23]

Quantification of FAAH activity with [11C]CURB was first performed by *ex vivo* biodistribution studies in rats.[18] High brain uptake (1.6–2.4 SUV, standardized uptake value) was followed by low washout, which is expected from an irreversible tracer. Radiotracer uptake was irreversible, consistent with known FAAH distribution,[24] and could be blocked by pretreatment with URB597 and other FAAH inhibitors. Human imaging studies showed rapid and high brain uptake of [11C]CURB with regional peak and plateau concentrations greatest in the putamen and thalamus compared to other regions,[22] matching human postmortem data.[25] A number of kinetic models were evaluated for accurate and reproducible FAAH quantification. A two-tissue compartment model with irreversible trapping was found to be optimal, and the composite parameter λk_3 provided a sensitive measure of FAAH activity.

While [11C]CURB appears to be a very promising radiotracer for FAAH, it is limited by the half-life of carbon-11 (11C, $t_{1/2}$ = 20.4 min), which necessitates an on-site cyclotron for radiotracer production and poses many practical challenges for its widespread use. In light of the potential demonstrated by [11C]CURB, a fluorine-18 (18F, $t_{1/2}$ = 109.7 min) labeled O-arylcarbamate, [18F]3-(4,5-dihydrooxazol-2-yl)phenyl (5-fluoropentyl)carbamate ([18F]DOPP), has been prepared in a three-step radiosynthesis and also evaluated in rats.[26] Similar to [11C]CURB, [18F]DOPP showed irreversible and specific binding, with regional distribution consistent with FAAH distribution. However, the stability of [18F]DOPP in rat plasma was low, as less than 5% of radioactivity was associated with the parent compound 5 min after radiotracer administration. Though the observed metabolism is likely associated with rodent carboxylesterases that are not present in human plasma,[27,28] rapid consumption of the parent radiotracer could have a profound effect on modeling outcome parameters of its distribution. In order to advance [18F]DOPP for human studies, we sought to evaluate the kinetics and metabolism of this radiotracer in higher species and with plasma input function correction. We are also interested in determining the sensitivity of [18F]DOPP binding by pretreatment with FAAH inhibitors in a dose dependent manner, prior to evaluation of this radiotracer in human subjects. In the present study, we conducted PET imaging of [18F]DOPP in nonhuman primates to assess brain uptake, washout, regional distribution, and kinetic modeling of this tracer following pretreatment studies.

■ EXPERIMENTAL SECTION

Synthesis. Precursors for the synthesis of [18F]DOPP were prepared by literature procedures with minor modifications.[26,29] Chemical yields and characterization data closely matched previously published values.

Radiochemistry. A GE PETtrace 16.5 MeV cyclotron was used for [18F]fluoride production by the $^{18}O(p,n)^{18}F$ nuclear reaction to irradiate 18O-enriched water. Synthesis of [18F]DOPP was performed manually using minor modifications to the previously reported automated procedure.[26] Specifically, [18F]fluoride drying was conducted as follows: A solution consisting of 14.4 mg of 4,7,13,16,21,24-hexaoxa-1,10-diazabicyclo[8.8.8]hexacosane (crypt-222), and 3 mg of K_2CO_3 in 1 mL of 10% (v/v) water in acetonitrile was used to elute [18F]fluoride from the ion-exchange resin and into a conical glass vial. The vented vial was heated to 90 °C under continuous nitrogen gas flow. When no liquid was visible in the vial, it was removed from heat, anhydrous acetonitrile (1 mL) was added, and the heating was resumed until dryness. This step was repeated an additional three times. The remainder of the radiosynthesis was conducted as previously described,[26] with the exceptions of reaction temperatures for [18F]fluoride incorporation and amine deprotection, which were increased to 100 °C from the previously reported 80 °C.

Drug Preparation. URB597 was purchased from Cayman Chemicals and formulated in saline with 5% ethanol and 5% Tween 80. All solutions were filtered through a 0.22 μm filter into a sterile empty vial and were tested for sterility and pyrogen content. An aliquot of the pretreatment solution for injection was withdrawn and analyzed by HPLC to determine URB597 concentration.

PET/MR Imaging. All animal studies were performed in accordance with the National Institutes of Health Guide for the Care and Use of Laboratory Animals and were approved by the Massachusetts General Hospital Institutional Animal Care and Use Committee.

Three adult baboons (*Papio anubis*, 2M/1F, 3–4 years old, 10.1–15.6 kg), deprived of food for 12 h prior to imaging experiments, were included in the study. One baseline and two pretreatment experiments were conducted for a total of three imaging sessions. Intramuscular ketamine (10 mg/kg) was

administered for animal preparation and intubation. Baboons were catheterized antecubitally for hydration and radiotracer injection, and a radial arterial line was placed for plasma and metabolite analysis. For maintenance of anesthesia throughout the imaging study, baboons were provided 1−2% isoflurane (Forane) in a mixture of medical oxygen. Body temperature was maintained by heated water blanket. Vital signs including end tidal CO_2, SpO_2, heart rate, respiration rate, and blood pressure were monitored and maintained within normal ranges during the studies.

PET and MRI images were acquired on a 3T Siemens TIM-Trio with a BrainPET insert (Siemens, Erlangen, Germany). A custom PET/MRI compatible 8-channel array coil for nonhuman primate brain imaging was used to improve image signal and quality. Dynamic PET image acquisition was initiated concurrently with the administration of the radiotracer (4.99 ± 0.20 mCi, 3 scans) in a homogeneous solution of 10% ethanol and 90% isotonic saline, and continued for a duration of 120 min. A high-resolution anatomical scan using multiecho MPRAGE sequence (TR = 2530 ms, TE1/TE2/TE3/TE4 = 1.64/3.5/5.36/7.22 ms, TI = 1200 ms, flip angle = 7°, and 1 mm isotropic) was acquired for anatomic coregistration. For pretreatment studies, baboons were administered URB597 (200 or 300 μg/kg, iv) 10 min prior to radiotracer administration.

Plasma and Metabolite Analysis. Blood was sampled from the radial arterial line nominally every 10 s for the first 3 min (~1 mL each) after radiotracer administration, followed by sampling at 5, 10, 20, 30, 45, 60, and 90 min time points (~3 mL each) for plasma and metabolite analysis. Arterial samples were centrifuged to obtain plasma, which was then removed (200 μL for samples collected during the first 3 min; 600 μL for all later samples) and placed in an automated gamma counter using a 350−600 keV window, and cross-calibrated with the PET scanner. Beginning with the arterial sample acquired at 5 min after radiotracer administration, an aliquot (600 μL) of plasma was added to acetonitrile (600 μL) and centrifuged for 1−3 min to obtain protein-free plasma (PFP). An aliquot (600 μL) of PFP was diluted with deionized water (3 mL) and loaded onto a customized automated robot, fitted with Phenomenex Strata-X 500 mg SPE cartridges that were primed with ethanol (2 mL) and deionized water (20 mL). Solutions of PFP were loaded on SPE cartridges and then extracted sequentially with 4 mL of 100% (twice), 90%, 85%, 80%, 75%, and 60% water, followed by 100% acetonitrile. This program had been previously tested with [18F]DOPP to determine its retention properties. Each eluent sample was counted in an automated gamma counter to determine the presence of radiolabeled metabolites.

Plasma Protein Binding. An aliquot of [18F]DOPP formulated in 10% ethanolic saline (10 μL) was added to a sample of baboon plasma (0.8 mL). The mixture was gently mixed by repeated inversion and incubated for 10 min at room temperature. Following incubation, a small sample (20 μL) was removed to determine the total radioactivity in the plasma sample (A_T; $A_T = A_{bound} + A_{unbound}$). An additional 0.2 mL of the plasma sample was placed in the upper compartment of a Centrifree ultrafiltration device (Amicon, Inc., Beverly, MA) and then centrifuged for 10 min. The upper part of the device and the membrane were discarded, and an aliquot (20 μL) from the collection cup was removed to determine the fraction of radioactivity that passed through the membrane ($A_{unbound}$).

Plasma protein binding is reported as the free fraction of radioactivity ($A_{unbound}/A_T$).

Data Analysis and Kinetic Modeling. PET data were registered to the Black baboon brain atlas[30] using JIP tools optimized for nonhuman primate data processing (www.nitrc.org/projects/jip). Image registration was carried out on high-resolution T_1-weighted anatomical MRI images using a 12 degree of freedom linear algorithm and a nonlinear algorithm to the atlas brain. The transformation was then applied to the simultaneously collected dynamic PET data.

Kinetic modeling was performed using PMOD 3.3 (PMOD Technologies Ltd., Zurich, Switzerland). Twelve volumes of interest (VOIs) were defined according to the Black baboon brain atlas.[30] Time−activity curves (TACs) were extracted from the amygdala (Amyg), dorsal lateral prefrontal cortex (DLPFC), hippocampus (HIP), primary motor cortex (M1), nucleus accumbens (NAc), posterior cingulate cortex (PCC), putamen (Put), orbitofrontal cortex (OFC), supplementary motor area (SMA), thalamus (Tha), caudate (Cau), and cerebellum (CB) VOIs for analysis. Compartmental models (one-tissue (1TCM), two-tissue (2TCM), and three-tissue (3TCM) compartmental models) with and without irreversible binding were carried out in PMOD using the metabolite-corrected arterial blood as input function. A composite parameter λk_3, where λ equals K_1/k_2, was determined for all VOIs from all scans and plotted in Figure 4. A two-way ANOVA was applied to compare regional λk_3 values between baseline and the two pretreatment scans using GraphPad Prism (Prism6, GraphPad Software Inc., La Jolla, CA, USA).

Because a 2TCM with irreversible binding (2TCMi) provides the best fits in regional analysis, voxelwise maps were then obtained using 2TCMi from the dynamic PET data using PMOD (PXMOD module). In order to implement a 2TCMi fitting on noisy voxelwise TACs, we implemented a published method to reduce the number of parameters being estimated.[31] Specifically, instead of fitting the model for voxelwise k_2, a K_1/k_2 ratio representing the distribution volume of free plus nonspecific binding of a high binding region (i.e., basal ganglia) was first estimated.[31] The resulting regional K_1/k_2 value was then held constant during voxelwise fitting.[31]

■ RESULTS AND DISCUSSION

Chemistry and Radiochemistry. [18F]DOPP was prepared by a multistep radiosynthesis that involved radiofluorination of a protected alkyl amine, deprotection, and coupling with a diaryl carbonate under buffered conditions to form the desired fluorine-18 labeled carbamate. Both the protected amine precursor and the diaryl carbonate precursor were prepared using literature procedures[26,29] with minor modifications. The synthesis of [18F]DOPP was adapted from the previously reported method,[26] which made use of an automated radiosynthesis module for synthesis and purification. In addition to a modified [18F]fluoride-drying procedure, in the manual synthesis both the radiofluorination and deprotection steps were conducted at slightly higher temperatures (100 °C compared to 80 °C). Specific activities in excess of 5.4 Ci·μmol^{-1} were obtained for the imaging studies.

PET/MR Imaging in Nonhuman Primate. After radiotracer injection, rapid brain uptake was observed in baboon brain at baseline by *in vivo* PET imaging (Figure 2A and Figure S1 in the Supporting Information). An initial whole-brain activity peak was observed at 45 s, and uptake reached a maximum of 2.1 SUV beginning at 55 min, with little washout
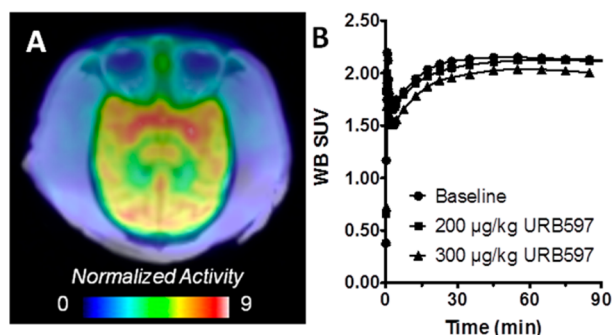
Figure 2. (A) Summed baseline PET/MR image 0−90 min post tracer injection. Image data is normalized to injected dose and animal weight (kBq/mL/mCi/kg). (B) Whole brain (WB) baboon time−activity curves for $[^{18}F]$DOPP at baseline and after pretreatment with URB597. Little change in uptake is observed in the summed PET images and time−activity curves after pretreatment. For summed PET/MR images after pretreatment, see the Supporting Information.

thereafter (Figure 2B). Regional uptake values for the plateau phase of the time−activity curves are greatest for the putamen and anterior cingulate cortex, reaching 2.8 SUV in each, and lowest in the temporal and occipital cortices, where peak activity was only 2.2 and 2.3 SUV, respectively. The nominal rank order was maintained both in the initial uptake peak and during the plateau phase.

URB597 is a carbamate-based inhibitor that, within the brain, is selective for FAAH.[32] Pretreatment of baboons with 200 or 300 μg/kg URB597 iv showed only modest reduction in whole brain radioactivity uptake at peak (1.8 SUV) and plateau (1.9 SUV) levels (Figure 2B and Figure S2 in the Supporting Information). The modest effect on radiotracer uptake likely reflects the opposing influences of increased delivery of $[^{18}F]$DOPP due to peripheral blocking (Figure 3, *vide infra*)
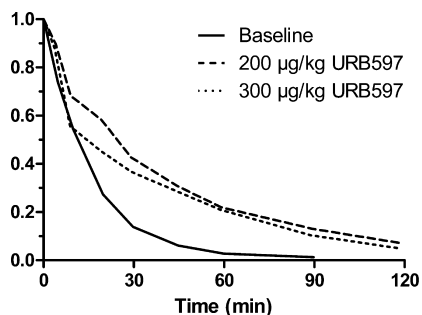

Figure 3. Parent fraction data from arterial plasma at baseline and after pretreatment at two different doses of URB597 (200 or 300 μg/kg iv). The rate of metabolism of $[^{18}F]$DOPP is rapid at baseline and significantly decreased by pretreatment with the FAAH inhibitor URB597.

and blocking of FAAH binding sites in the central nervous system (CNS). There is scant literature on higher doses of URB597 administered intravenously to nonhuman primates,[33] and given the complete blocking observed in rat,[26] experimental higher dosing regimens were not considered to be justified in the present study. The limited whole brain blocking of FAAH observed in nonhuman primates at this level of pretreatment with URB597 also provides an excellent opportunity to evaluate the sensitivity of $[^{18}F]$DOPP and kinetic modeling approaches to quantification of FAAH with

high sensitivity. Selectivity of $[^{18}F]$DOPP for FAAH has been previously demonstrated in rats using relatively high doses of URB597 (2 mg/kg), or a more potent urea-based FAAH inhibitor, PF-04457845.[26]

Plasma and Metabolite Analysis. Plasma protein binding was measured at 3.9% free fraction. This compares favorably with $[^{11}C]$CURB in humans, where free fraction in plasma was estimated at 0.9%.[22] Unmetabolized $[^{18}F]$DOPP in arterial plasma peaked at 11.9 SUV, 40 s after radiotracer administration, and declined to 2.0 SUV after just 3 min and to 0.05 SUV at 70 min postinjection (see Figure S3, Supporting Information). Metabolism of $[^{18}F]$DOPP *in vivo* was rapid. Less than 5% of radioactivity in plasma was associated with the parent compound at 50 min postadministration (Figure 3). Following pretreatment with URB597 (300 μg/kg, iv), $[^{18}F]$DOPP in arterial plasma peaked at 13.1 SUV at 29 s and declined to 2.0 SUV at 3.7 min and to 0.05 SUV at 71 min. The observed slight increase in plasma concentration at early time points after pretreatment is consistent with moderate blocking of FAAH in the brain as well as peripheral metabolic enzymes.[27,32] Indeed, the stability of $[^{18}F]$DOPP *in vivo* was significantly augmented after pretreatment with URB597. By way of comparison with baseline, at 50 min postadministration, 26% of radioactivity was associated with the parent compound under pretreatment conditions. Metabolism of the parent compound did not reach 95% until approximately 113 min postinjection. This confirms our previous hypothesis that the rapid peripheral metabolism of $[^{18}F]$DOPP observed in rodents would not translate to higher species.[26]

Kinetic Modeling. To determine the optimal kinetic parameters for FAAH quantification using $[^{18}F]$DOPP, a number of different tissue-compartment models (TCMs) were evaluated with the data from a baseline scan and two pretreatment scans (URB597, 200, and 300 μg/kg iv, 10 min prior to radiotracer administration). These included 1TCM, 2TCMs, and 3TCMs with and without irreversible trapping. Consistent with a previous human study,[22] the 2TCMi was found to give a good fit for the data in all scans. The 3TCMi did not outperform the 2TCMi as judged by the percent errors of the fits and resulted in comparable outcome measurements. The composite parameter λk_3 was used to quantify FAAH activity in regional VOIs. The regional λk_3 values at baseline ranged from 0.09 to 0.16 mL/cm^3/min (Figure 4). By way of
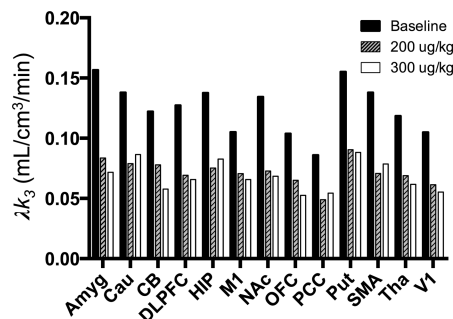
Figure 4. Regional brain λk_3 values for baseline and at both pretreatment doses with URB597. Amyg, amygdala; Cau, caudate; CB, cerebellum; DLPFC, dorsal lateral prefrontal cortex; HIP, hippocampus; M1, primary motor cortex; NAc, nucleus accumbens; OFC, orbitofrontal cortex; PCC, posterior cingulate cortex; Put, putamen; SMA, supplementary motor area; Tha, thalamus; V1, primary visual cortex.

comparison, the average λk_3 value for $[^{11}C]$CURB in selected human brain regions was 0.14 mL/cm^3/min.[22] The trend and rank order of regional λk_3 values also correspond well with previously reported human imaging analysis with $[^{11}C]$CURB. Regional λk_3 values showed significant reduction of FAAH binding when comparing both pretreatment scans to baseline condition (one-way ANOVA with Tukey correction for multiple comparisons, $p < 0.0001$), while the two pretreatment doses did not cause different levels of blockade ($p > 0.05$). However, trends of dose-dependent blocking are evident for most brain structures evaluated. Putamen and amygdala showed the highest λk_3 at baseline, while cortical regions such as occipital (V1) and motor (M1) cortices had the lowest values. Across brain regions, λk_3 values were reduced by 42.2 ± 4.5% by pretreatment with 200 µg/kg URB597, and by 45.1 ± 6.0% at the 300 µg/kg level.

As a 3TCMi would significantly increase the complexity and computational burden of generating voxelwise maps, the 2TCMi was used to generate voxelwise maps. Figure 5 shows
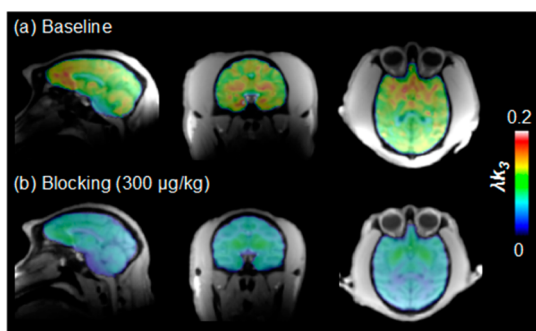
Figure 5. Nonhuman primate brain λk_3 maps overlaid on their anatomical MRI (a) at baseline and (b) after pretreatment with 300 µg/kg URB597.

the voxelwise λk_3 maps overlaid on their high-resolution anatomical MRI under baseline conditions and with 300 µg/kg pretreatment. In accordance to regional analysis, basal ganglia (in particular the putamen) and the amygdala show the highest FAAH activity.

Among the challenges of developing irreversible covalent enzyme inhibitors for PET are achieving selectivity for the enzyme target and a rate of enzyme inhibition that is not limited by flow. Pretreatment studies with FAAH inhibitors prior to administration of either $[^{11}C]$CURB[18] or $[^{18}F]$DOPP[26] have shown that both of these radiotracers exhibit high selectivity for FAAH. Human studies with $[^{11}C]$CURB have also proven that FAAH activity as quantified by this radiotracer is not dependent on cerebral blood flow.[22] Although the potential effects of cerebral blood flow were not directly measured in the present study, it is possible to use the values of microparameters derived from kinetic modeling to assess whether tracer distribution is flow-limited. Specifically, the ratio of k_3/k_2 has been proposed as a useful metric for this purpose, and values within the range of 0.1−0.3 are predictive of an optimal balance of high tracer uptake without flow-limited distribution.[31] Since a high k_3 is indicative of rapid specific binding, a value above this range is suggested to indicate flow dependence, while a value below this range will likely translate to poor uptake and low signal. Over all of the ROIs analyzed, the mean k_3/k_2 value was 0.18, which is within the optimal range.

Since $[^{18}F]$DOPP is an irreversible inhibitor of FAAH, PET measurements with this compound provide a measure of enzyme *activity*, as opposed to enzyme *availability*, which could be measured with reversible inhibitors in the same manner as a ligand−receptor interaction.[34] The effects of anesthesia are known to play a role in PET imaging of G protein coupled receptors and enzyme targets in the CNS.[35] The effects of isoflurane anesthesia used in the present study, as necessary for imaging in nonhuman primates, present a potential confounding factor for translation of $[^{18}F]$DOPP for quantification of FAAH activity in conscious humans.

CONCLUSIONS

In summary, we report that $[^{18}F]$DOPP rapidly crosses the nonhuman primate blood−brain barrier and shows low washout in regions consistent with FAAH distribution and the distribution of $[^{11}C]$CURB in human brain imaging studies. We further report on the evaluation of kinetic modeling parameters and found that λk_3 displays sensitivity to pretreatment with a FAAH inhibitor, URB597. As predicted, $[^{18}F]$DOPP is rapidly metabolized *in vivo* and at a reduced rate after pretreatment with URB597. In combination with the previously reported data in rats,[26] these data are suggestive that $[^{18}F]$DOPP exhibits high specific binding and that distribution is not flow dependent, attributes that will ultimately be characterized in human subjects. The radiosynthesis of $[^{18}F]$DOPP has been validated for human use, and preparations for clinical research studies are underway.

ASSOCIATED CONTENT

Ⓢ **Supporting Information**
Summed PET/MR images for baseline and pretreatment imaging experiments, Figures S1 and S2. Metabolite-corrected plasma time−activity curves, Figure S3. This material is available free of charge via the Internet at http://pubs.acs.org.

AUTHOR INFORMATION

Corresponding Authors
*E-mail: hooker@nmr.mgh.harvard.edu.
*E-mail: vasdev.neil@mgh.harvard.edu.
Notes
The authors declare no competing financial interest.

ACKNOWLEDGMENTS

ABBREVIATIONS USED

2-AG, 2-arachidonoylglycerol; CB$_1$, cannabinoid receptor 1; CB$_2$, cannabinoid receptor 2; CNS, central nervous system; FAAH, fatty acid amide hydrolase; MAGL, monoacylglycerol lipase; PET/MR, positron emission tomography−magnetic

resonance imaging; SUV, standardized uptake value; TCM, tissue-compartment model; VOI, volume of interest

■ REFERENCES

(1) Piomelli, D. The Molecular Logic of Endocannabinoid Signalling. *Nat. Rev. Neurosci.* **2003**, *4*, 873−884.

(2) Ahn, K.; McKinney, M. K.; Cravatt, B. F. Enzymatic Pathways That Regulate Endocannabinoid Signaling in the Nervous System. *Chem. Rev.* **2008**, *108*, 1687−1707.

(3) Alger, B. E.; Kim, J. Supply and Demand for Endocannabinoids. *Trends Neurosci.* **2011**, *34*, 304−315.

(4) Fowler, C. J. The Cannabinoid System and Its Pharmacological Manipulation − a Review, with Emphasis upon the Uptake and Hydrolysis of Anandamide. *Fundam. Clin. Pharmacol.* **2006**, *20*, 549−562.

(5) Fowler, C. J. Anandamide Uptake Explained? *Trends Pharmacol. Sci.* **2012**, *33*, 181−185.

(6) Di Marzo, V. Targeting the Endocannabinoid System: To Enhance or Reduce? *Nat. Rev. Drug Discovery* **2008**, *7*, 438−455.

(7) Blankman, J. L.; Cravatt, B. F. Chemical Probes of Endocannabinoid Metabolism. *Pharmacol. Rev.* **2013**, *65*, 849−871.

(8) Kathuria, S.; Gaetani, S.; Fegley, D.; Valiño, F.; Duranti, A.; Tontini, A.; Mor, M.; Tarzia, G.; Rana, G. L.; Calignano, A.; Giustino, A.; Tattoli, M.; Palmery, M.; Cuomo, V.; Piomelli, D. Modulation of Anxiety through Blockade of Anandamide Hydrolysis. *Nat. Med.* **2003**, *9*, 76−81.

(9) Johnson, D. S.; Stiff, C.; Lazerwith, S. E.; Kesten, S. R.; Fay, L. K.; Morris, M.; Beidler, D.; Liimatta, M. B.; Smith, S. E.; Dudley, D. T.; Sadagopan, N.; Bhattachar, S. N.; Kesten, S. J.; Nomanbhoy, T. K.; Cravatt, B. F.; Ahn, K. Discovery of PF-04457845: A Highly Potent, Orally Bioavailable, and Selective Urea FAAH Inhibitor. *ACS Med. Chem. Lett.* **2011**, *2*, 91−96.

(10) Ahn, K.; Smith, S. E.; Liimatta, M. B.; Beidler, D.; Sadagopan, N.; Dudley, D. T.; Young, T.; Wren, P.; Zhang, Y.; Swaney, S.; Van Becelaere, K.; Blankman, J. L.; Nomura, D. K.; Bhattachar, S. N.; Stiff, C.; Nomanbhoy, T. K.; Weerapana, E.; Johnson, D. S.; Cravatt, B. F. Mechanistic and Pharmacological Characterization of PF-04457845: A Highly Potent and Selective Fatty Acid Amide Hydrolase Inhibitor That Reduces Inflammatory and Noninflammatory Pain. *J. Pharmacol. Exp. Ther.* **2011**, *338*, 114−124.

(11) Li, G. L.; Winter, H.; Arends, R.; Jay, G. W.; Le, V.; Young, T.; Huggins, J. P. Assessment of the Pharmacology and Tolerability of PF-04457845, an Irreversible Inhibitor of Fatty Acid Amide Hydrolase-1, in Healthy Subjects: Pharmacology and Tolerability of PF-04457845. *Br. J. Clin. Pharmacol.* **2012**, *73*, 706−716.

(12) Huggins, J. P.; Smart, T. S.; Langman, S.; Taylor, L.; Young, T. An Efficient Randomised, Placebo-Controlled Clinical Trial with the Irreversible Fatty Acid Amide Hydrolase-1 Inhibitor PF-04457845, Which Modulates Endocannabinoids but Fails to Induce Effective Analgesia in Patients with Pain due to Osteoarthritis of the Knee. *Pain* **2012**, *153*, 1837−1846.

(13) wyffels, L.; Muccioli, G. G.; De Bruyne, S.; Moerman, L.; Sambre, J.; Lambert, D. M.; De Vos, F. Synthesis, In Vitro and In Vivo Evaluation, and Radiolabeling of Aryl Anandamide Analogues as Candidate Radioligands for In Vivo Imaging of Fatty Acid Amide Hydrolase in the Brain. *J. Med. Chem.* **2009**, *52*, 4613−4622.

(14) Hicks, J. W.; Parkes, J.; Sadovski, O.; Tong, J.; Houle, S.; Vasdev, N.; Wilson, A. A. Synthesis and Preclinical Evaluation of [11C-carbonyl]PF-04457845 for Neuroimaging of Fatty Acid Amide Hydrolase. *Nucl. Med. Biol.* **2013**, *40*, 740−746.

(15) Skaddan, M. B.; Zhang, L.; Johnson, D. S.; Zhu, A.; Zasadny, K. R.; Coelho, R. V.; Kuszpit, K.; Currier, G.; Fan, K.-H.; Beck, E. M.; Chen, L.; Drozda, S. E.; Balan, G.; Niphakis, M.; Cravatt, B. F.; Ahn, K.; Bocan, T.; Villalobos, A. The Synthesis and In Vivo Evaluation of [18F]PF-9811: A Novel PET Ligand for Imaging Brain Fatty Acid Amide Hydrolase (FAAH). *Nucl. Med. Biol.* **2012**, *39*, 1058−1067.

(16) Liu, P.; Hamill, T. G.; Chioda, M.; Chobanian, H.; Fung, S.; Guo, Y.; Chang, L.; Bakshi, R.; Hong, Q.; Dellureficio, J.; Lin, L. S.; Abbadie, C.; Alexander, J.; Jin, H.; Mandala, S.; Shiao, L.-L.; Li, W.; Sanabria, S.; Williams, D.; Zeng, Z.; Hajdu, R.; Jochnowitz, N.; Rosenbach, M.; Karanam, B.; Madeira, M.; Salituro, G.; Powell, J.; Xu, L.; Terebetski, J. L.; Leone, J. F.; Miller, P.; Cook, J.; Holahan, M.; Joshi, A.; O'Malley, S.; Purcell, M.; Posavec, D.; Chen, T.-B.; Riffel, K.; Williams, M.; Hargreaves, R.; Sullivan, K. A.; Nargund, R. P.; DeVita, R. J. Discovery of MK-3168: A PET Tracer for Imaging Brain Fatty Acid Amide Hydrolase. *ACS Med. Chem. Lett.* **2013**, *4*, 509−513.

(17) wyffels, L.; Muccioli, G. G.; Kapanda, C. N.; Labar, G.; De Bruyne, S.; De Vos, F.; Lambert, D. M. PET Imaging of Fatty Acid Amide Hydrolase in the Brain: Synthesis and Biological Evaluation of an 11C-Labelled URB597 Analogue. *Nucl. Med. Biol.* **2010**, *37*, 665−675.

(18) Wilson, A. A.; Garcia, A.; Parkes, J.; Houle, S.; Tong, J.; Vasdev, N. [11C]CURB: Evaluation of a Novel Radiotracer for Imaging Fatty Acid Amide Hydrolase by Positron Emission Tomography. *Nucl. Med. Biol.* **2011**, *38*, 247−253.

(19) Wilson, A. A.; Hicks, J. W.; Sadovski, O.; Parkes, J.; Tong, J.; Houle, S.; Fowler, C. J.; Vasdev, N. Radiosynthesis and Evaluation of [11C-carbonyl]-Labeled Carbamates as Fatty Acid Amide Hydrolase Radiotracers for Positron Emission Tomography. *J. Med. Chem.* **2013**, *56*, 201−209.

(20) Rotstein, B. H.; Liang, S. H.; Holland, J. P.; Collier, T. L.; Hooker, J. M.; Wilson, A. A.; Vasdev, N. 11CO2 Fixation: A Renaissance in PET Radiochemistry. *Chem. Commun.* **2013**, *49*, 5621−5629.

(21) Joshi, A.; Li, W.; Sanabria, S.; Holahan, M.; Purcell, M.; Declercq, R.; Depre, M.; Bormans, G.; Van Laere, K.; Hamill, T. Translational Studies with [11C]MK-3168, a PET Tracer for Fatty Acid Amide Hydrolase (FAAH). *Soc. Nucl. Med. Annu. Meet. Abstr.* **2012**, *53*, 397.

(22) Rusjan, P. M.; Wilson, A. A.; Mizrahi, R.; Boileau, I.; Chavez, S. E.; Lobaugh, N. J.; Kish, S. J.; Houle, S.; Tong, J. Mapping Human Brain Fatty Acid Amide Hydrolase Activity with PET. *J. Cereb. Blood Flow Metab.* **2012**, *33*, 407−414.

(23) Alexander, J. P.; Cravatt, B. F. Mechanism of Carbamate Inactivation of FAAH: Implications for the Design of Covalent Inhibitors and In Vivo Functional Probes for Enzymes. *Chem. Biol.* **2005**, *12*, 1179−1187.

(24) Ueda, N.; Puffenbarger, R. A.; Yamamoto, S.; Deutsch, D. G. The Fatty Acid Amide Hydrolase (FAAH). *Chem. Phys. Lipids* **2000**, *108*, 107−121.

(25) Romero, J.; Hillard, C. J.; Calero, M.; Rabano, A. Fatty Acid Amide Hydrolase Localization in the Human Central Nervous System: An Immunohistochemical Study. *Mol. Brain Res.* **2002**, *100*, 85−93.

(26) Sadovski, O.; Hicks, J. W.; Parkes, J.; Raymond, R.; Nobrega, J.; Houle, S.; Cipriano, M.; Fowler, C. J.; Vasdev, N.; Wilson, A. A. Development and Characterization of a Promising Fluorine-18 Labelled Radiopharmaceutical for In Vivo Imaging of Fatty Acid Amide Hydrolase. *Bioorg. Med. Chem.* **2013**, *21*, 4351−4357.

(27) Zhang, D.; Saraf, A.; Kolasa, T.; Bhatia, P.; Zheng, G. Z.; Patel, M.; Lannoye, G. S.; Richardson, P.; Stewart, A.; Rogers, J. C.; Brioni, J. D.; Surowy, C. S. Fatty Acid Amide Hydrolase Inhibitors Display Broad Selectivity and Inhibit Multiple Carboxylesterases as off-Targets. *Neuropharmacology* **2007**, *52*, 1095−1105.

(28) Li, B.; Sedlacek, M.; Manoharan, I.; Boopathy, R.; Duysen, E. G.; Masson, P.; Lockridge, O. Butyrylcholinesterase, Paraoxonase, and Albumin Esterase, but Not Carboxylesterase, Are Present in Human Plasma. *Biochem. Pharmacol.* **2005**, *70*, 1673−1684.

(29) Lustoň, J.; Kronek, J.; Böhme, F. Synthesis and Polymerization Reactions of Cyclic Imino Ethers. I. Ring-Opening Homopolyaddition of AB-Type Hydroxyphenyl-Substituted 2-Oxazolines. *J. Polym. Sci., Part A: Polym. Chem.* **2006**, *44*, 343−355.

(30) Black, K. J.; Snyder, A. Z.; Koller, J. M.; Gado, M. H.; Perlmutter, J. S. Template Images for Nonhuman Primate Neuro-imaging: 1. Baboon. *NeuroImage* **2001**, *14*, 736−743.

(31) Koeppe, R. A.; Frey, K. A.; Snyder, S. E.; Meyer, P.; Kilbourn, M. R.; Kuhl, D. E. Kinetic Modeling of N-[11C]Methylpiperidin-4-yl Propionate: Alternatives for Analysis of an Irreversible Positron Emission Tomography Tracer for Measurement of Acetylcholinester-

ase Activity in Human Brain. *J. Cereb. Blood Flow Metab.* **1999**, *19*, 1150−1163.

(32) Lichtman, A. H.; Leung, D.; Shelton, C. C.; Saghatelian, A.; Hardouin, C.; Boger, D. L.; Cravatt, B. F. Reversible Inhibitors of Fatty Acid Amide Hydrolase That Promote Analgesia: Evidence for an Unprecedented Combination of Potency and Selectivity. *J. Pharmacol. Exp. Ther.* **2004**, *311*, 441−448.

(33) Stewart, J. L.; McMahon, L. R. The Fatty Acid Amide Hydrolase Inhibitor URB 597: Interactions with Anandamide in Rhesus Monkeys. *Br. J. Pharmacol.* **2011**, *164*, 655−666.

(34) Cumming, P.; Vasdev, N. The Assay of Enzyme Activity by Positron Emission Tomography. In *Molecular Imaging in the Clinical Neurosciences*; Gründer, G., Ed.; Humana Press: Totowa, NJ, 2012; Vol. *71*, pp 111−135.

(35) Alstrup, A. K. O.; Smith, D. F. Anaesthesia for Positron Emission Tomography Scanning of Animal Brains. *Lab. Anim.* **2013**, *47*, 12−18.